

# Multi-GHz repetition rate, multi-watt average power, ultraviolet laser pulses for fast trapped-ion entanglement operations

M. I. Hussain,<sup>1, 2</sup> \* D. Heinrich,<sup>1, 2</sup> M. Guevara-Bertsch,<sup>1, 2</sup> E. Torrontegui,<sup>3</sup> J. J. García-Ripoll,<sup>3</sup> C. F. Roos,<sup>1, 2</sup> and R. Blatt<sup>1, 2</sup>

<sup>1</sup>*Institute for Quantum Optics and Quantum Information (IQOQI), Austrian Academy of Sciences, Innsbruck 6020, Austria*

<sup>2</sup>*Institute for Experimental Physics, University of Innsbruck 6020, Austria*

<sup>3</sup>*Instituto de Física Fundamental IFF-CSIC, Calle Serrano 113b, 28006 Madrid, Spain*

The conventional approach to perform two-qubit gate operations in trapped ions relies on exciting the ions on motional sidebands with laser light, which is an inherently slow process. One way to implement a fast entangling gate protocol requires a suitable pulsed laser to increase the gate speed by orders of magnitude. However, the realization of such a fast entangling gate operation presents a big technical challenge, as such the required laser source is not available off-the-shelf. For this, we have engineered an ultrafast entangling gate source based on a frequency comb. The laser generates bursts of several hundred mode-locked pulses with pulse energy  $\sim 800$  pJ at 5 GHz repetition rate at 393.3 nm and complies with all requirements for implementing a fast two-qubit gate operation. To verify the applicability and projected performance we run simulations based on our source parameters. The gate time can be faster than a trap period with an error approaching  $10^{-4}$ .

PACS numbers:

## I. INTRODUCTION

Trapped atomic ions are a well-known resource for testing and implementing quantum information and quantum computation protocols [1–5]. One of the challenges to execute complex quantum algorithms is to increase the number of gate operations that can be carried out within the coherence time of the ion. Given a fixed coherence time, developing faster gate operations is a promising strategic approach to address the aforementioned problem. Well-established and routinely used entangling gate schemes depend on the Coulomb-coupled normal-modes of motion of the ions [6, 7]. The typical time-scale of the motional modes of the ion is on the order of microseconds, posing a restriction on the speed of the entangling gate operation. Therefore, implementing faster entangling gate schemes will be a major advancement towards scalable quantum computing. In this pursuit, a scheme was proposed by García-Ripoll [8] which exploits state-dependent momentum kicks rather than spectrally resolved motional sidebands to realize a two-qubit entangling gate operation faster than the motional mode period.

The idea is to expose the ion to counter-propagating resonant laser pulses, where each pulse provides a state-dependent momentum kick on the ion by coherent population transfer between the ground and an excited state. The momentum kicks drive the motional modes of the ions and, given precise control over the timing of incident pulses, force the modes to follow a closed trajectory which creates a relative phase between qubit states to generate

entanglement [8]. The fast gate scheme does not rely on resolving motional sidebands and hence can be completed in less than a trap period. Attempts are being made to realize fast gate operations by a number of research groups [9–12]. Rydberg-mediated entangling gate operations have been proven as a route towards faster gate operations: a two-qubit gate time of 700 ns is achieved to generate a Bell state with 78% fidelity [12]. A recent study reported the use of amplitude-modulated pulses for producing a two-qubit gate with a gate time of 480 ns [11]. Non-resonant Raman ultraviolet (UV) pulses were used to excite a single trapped-ion [9, 10] and a proof-of-principle demonstration of a two-qubit phase gate with a gate time greater than the trap period has been reported outside the Lamb-Dicke regime, i.e., the gate operation is insensitive to the thermal motional state of the ions [13].

There are ongoing efforts to develop high average power and high repetition rate, ultrafast UV and extreme-UV laser sources [14–18] for a range of applications and particularly for quantum computation to expedite entangling gates in trapped ions [19]. In the latter, the difficulty lies in achieving a higher repetition rate ( $\gg 1/\text{trap period}$ ) and sufficiently high pulse energy to enable state-dependent kicks, while restricting the wavelength range to a specific narrow-band ultraviolet spectrum.

In the present work, we generate frequency-quadrupled UV, picosecond laser pulses for fast entangling gate operations in trapped  $^{40}\text{Ca}^+$  ions. The center frequency of the laser source resonates with a strong atomic dipole transition (393 nm) in  $^{40}\text{Ca}^+$ . The pulse duration ( $\sim 1$  ps) is much shorter than the excited state lifetime (6.9 ns) of the ion in order to suppress spontaneous emission. The combination of a high repetition rate of 5 GHz and a fast

\*Electronic address: mahmood.hussain@uibk.ac.at

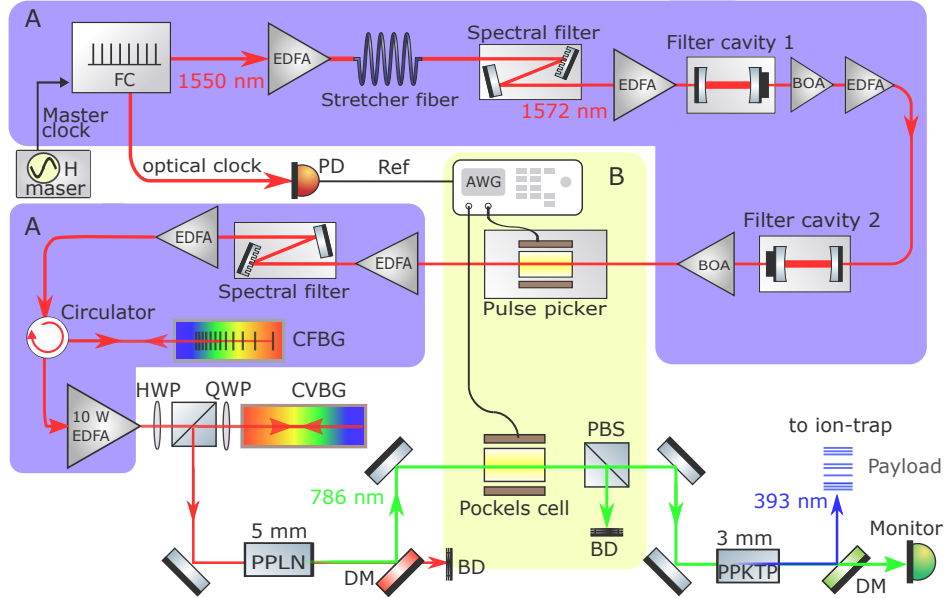


FIG. 1: Schematic of the ultrafast pulsed laser source. (A) The colour panels (purple) represent mostly the in-fiber part of the laser system. In these sections, chirped laser pulses at 5 GHz repetition rate are created with the right optical spectrum to reach the desired wavelength for high power amplification. Subsequently, amplified pulses travel through free space where nearly transform-limited pulse compression is achieved in CVBG and frequency up-conversion takes place via two non-linear crystals. (B) The yellow panel depicts our pulse-switching scheme in infrared and visible wavelengths. Black arrows/lines correspond to electronic signals. AWG: arbitrary waveform generator, BD: beam dump, BOA: booster optical amplifier CFBG: chirped fiber Bragg grating CVBG: chirped volume Bragg grating, DM: dichroic mirror, EDFA: erbium-doped fiber amplifier, FC: optical frequency comb, HWP: half-wave plate PBS: polarizing beam splitter, PD: photo detector, PPLN: periodically poled lithium niobate, PPKTP: periodically poled potassium titanyl phosphate, QWP: quarter-wave plate, H maser: passive hydrogen maser.

pulse picker provides precise control over the timing of picked pulses relative to the ion motion. At 5 GHz repetition rate, bursts of a few hundred of UV laser pulses are generated with an estimated average power of 5 W. At a reduced pulse repetition rate of 1.25 GHz, we estimate an average power of over 1 W. In both cases, the corresponding pulse energy is roughly 10 times more than previously utilized for a coherent population transfer with a probability of over 90% [20]. This enhanced pulse energy allows us to comfortably distribute the pulse energy for inducing counter-propagating kicks on the ions.

The paper is structured as follows: In section II we briefly describe the fundamental oscillator and related components that seed the laser source. Section III explains the single pulse switching of 5 GHz fast laser pulses to create pulse sequences for the implementation of a gate. The methods and generation of UV pulses is thoroughly discussed in section IV. Numerical simulations have been carried out based on our source parameters detailed in section V. Finally, we conclude the paper in section VI.

## II. 5 GHz TELECOM BAND FREQUENCY COMB

The seed oscillator is based on a fiber laser frequency comb produced by Menlo Systems. The mode-locked erbium-doped fiber cavity produces 75 fs laser pulses at a center wavelength of 1550 nm with a fundamental repetition rate of 250 MHz. A passive hydrogen maser serves as a master clock with a fractional frequency instability of  $\leq 9 \times 10^{-15}/\text{hr}$  to lock the carrier-envelope offset and laser pulse repetition rate. Multiple erbium-doped fiber amplifiers (EDFAs) and booster optical amplifiers (BOAs) have been installed to compensate for insertion losses at various points in the laser set-up. Laser pulses out of the seed oscillator are amplified in the first pre-EDFA and chirped by the stretcher fiber as shown in panel A of Fig. 1. Chirped pulses travel through a spectral filter where the spectral bandwidth is reduced to 8 nm with a new center wavelength of 1572 nm ( $4 \times 393$  nm). The repetition rate is ramped up to 5 GHz by a filter cavity with a free spectral range such that it transmits only spectral modes spaced 5 GHz apart and suppresses all others. The same process is repeated in the second filter cavity to increase the extinction ratio between trans-

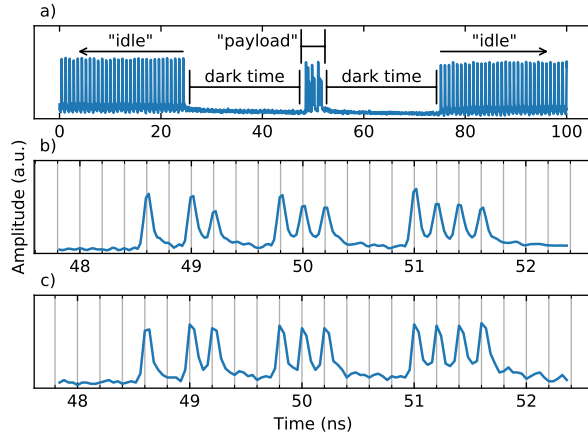


FIG. 2: Fast photodiode trace of residual 786 nm laser pulses exiting the PPKTP crystal. (a) An arbitrary pulse pattern is created with the pulse picker at 1572 nm wavelength. (b) Picking only the payload by using both pulse picker and Pockels cell. Here, the BOA amplifies the pulses after the pulse picker to feed the forthcoming stage in the laser setup. (c) Same as (b), but the BOA is replaced by an EDFA. Now, all transmitted pulses have the same amplitude. Every grid line in the insets of (b) and (c) shows the location of a pulse in the 5 GHz continuous pulse train. Figures (a) and (b) are adapted from [20].

mitted and suppressed comb modes. We integrate a BOA after the second filter cavity to reduce the pulse-to-pulse amplitude noise by saturating the amplifier [21]. Both cavities are locked to an auxiliary continuous-wave laser which in turn is locked to a mode of the frequency comb as detailed in reference [22].

### III. PULSE PATTERNING

To convert our pulsed laser into a fast entangling gate source, the device has to be capable of making pulse patterns by switching individual laser pulses. For its realization, we employ two switching stages synchronized with a 250 MHz optical clock extracted directly from the frequency comb as shown in Fig. 1. Single-pulse switching is done in the first stage inside a pulse picker (Photoline), constituted of a Mach-Zehnder interferometer and an electro-optic-modulator with 7 GHz bandwidth that is driven by an arbitrary waveform generator with a data rate of 25 GS/s. The fast pulse picker creates a *payload signal* by picking individual pulses at 1572 nm as shown in Fig. 2a. In order to seed subsequent amplifiers, the pulse picker transmits a continuous pulse train at all other times, the *idle signal*. The second stage is a barium borate Pockels cell that serves as a slow switch with a minimum allowed switching time of 35 ns to filter the payload pulses by blocking the idle signal. Previously [20], we observed that a pulse succeeding a blocked pulse—i.e., a dark time—had a different phase and amplitude

with respect to a pulse succeeding a transmitted pulse as shown in Fig. 2b. We found that the BOA (which was installed right after the pulse picker) was responsible for these anomalies because the carrier injection and recombination time of such amplifiers is similar to the 200 ps pulse period [23] of the pulse train. The effective gain recovery time  $\tau_g$  of this BOA was measured to be  $\leq 500$  ps. This is the reason why the pulse anomalies were prominent at 5 GHz repetition rate (see Fig. 3a) and disappeared at 1.25 GHz. The pulse repetition rate is changed by picking individual pulses inside the pulse picker.

To overcome the aforementioned problem, a seemingly straightforward solution is to establish a sufficiently fast gain recovery ( $\tau_g \ll 200$  ps) during amplification. However, we could not find an easy solution for achieving such amplification at 5 GHz repetition rate that was compatible with our local pre-amplification laser parameters. On the other hand, we find that integrating an amplifier with a much slower gain recovery time i.e.,  $\tau_g \gg 200$  ps can make the amplification immune to the fast changes due to a high repetition rate. Therefore, we substituted the BOA with a suitable EDFA with  $\tau_g$  on the order of microseconds.

The potential pulse-to-pulse phase shifts are verified and quantified by interfering the pulses in a Michelson interferometer [22]. The beam splitter divides the payload pulses into two beams. One of the beams is time-delayed by one pulse period  $\tau_{\text{pulse}}$  with respect to the other one before the beams are recombined on the interferometer's beam splitter. In this way, every pulse  $i$  interferes with the successive pulse  $i + 1$  in the payload. The interference signals are recorded by a fast photodiode. The net phase difference  $\Delta\Phi_i$  of the two pulses at the output of the interferometer is a function of the phase difference  $\Delta\phi_i$  of the interfering pulses, and the path length difference  $\Delta x = 2(x_2 - x_1) = c \cdot \tau_{\text{pulse}}$  and  $\Delta\Phi_i = \Delta\phi_i + k \cdot \Delta x$ , where  $x_1$  and  $x_2$  are the lengths of interferometer arms,  $c$  is the speed of light and  $k$  the magnitude of the wave vector.

### IV. UV PULSE GENERATION

In contrast to all previous stages (see the Fig. 1 panels A and B), high peak intensities are required for non-linear frequency conversion in order to maximize the output power. However, given a constant average power, an increase in the repetition rate reduces peak intensity, which deteriorates the conversion process and forces us to make a trade-off between repetition rate and peak intensity. To this end, we (a) maximize the amplification as much as available (10 W EDFA) with all desired laser parameters at 1572 nm, (b) minimize losses during post-amplification dechirping, and (c) efficiently remove dispersion to attain bandwidth-limited pulses.

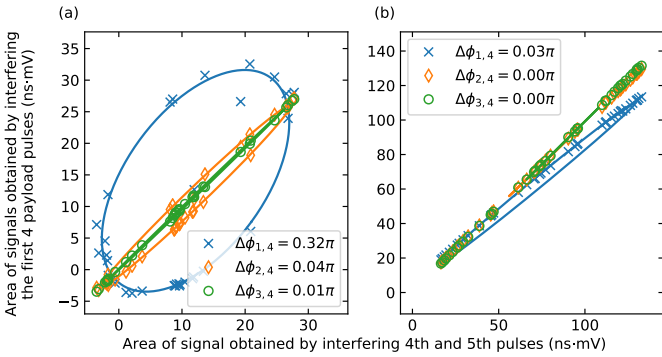


FIG. 3: Fitting fast photodiode data to measure relative phase shifts in the first 5 consecutive payload pulses at 5 GHz. These 5 pulses are sent to a Michelson interferometer such that each pulse interferes with its predecessor. We measure the subsequent 4 interferometric pulses with a fast photodiode and extract the measured pulse area of each with an oscilloscope. In the figure, the area of the first 3 interferometric pulses (blue crosses, yellow diamonds, green circles, respectively) is plotted against the area of the 4th pulse. By changing the optical path length difference of the interferometer on the order of  $\delta$ , where  $\lambda \lesssim \delta \ll c \cdot \tau$ , i.e., only small changes on the order of the wavelength and much less than the spacial pulse separation, we obtain data points which lie on an ellipse or a line segment. (a) Fitting an ellipse to our data allows us to extract the phase shifts between the 1st & 2nd, 2nd & 3rd, and 3rd & 4th pulses relative to the phase shift between the 4th & 5th pulses. This data was taken when BOA was a part of the (old) setup. (b) Same as (a), but the BOA has been replaced with an EDFA.

### A. Dispersion control

In order to satisfy (a), dispersion management in the laser system is crucial for achieving amplification that is free of self-phase-modulation (SPM). We estimate the dispersion required to avoid inducing non-linearity in the high power EDFA to be  $|D_\lambda| \sim 12.5$  ps/nm. We optimize dispersion by adding and removing chirp in three stages: First, we add a chirped fiber Bragg grating (CFBG, made by TeraXion) just before the high power amplifier. The CFBG provides a dispersion of -9.5 ps/nm. Next, a chirped volume Bragg grating (CVBG, produced by OptiGrate), which adds +12.5 ps/nm of dispersion, is set up in the free-space output of the 10 W EDFA. In the last step, we carefully balance the dispersion by adjusting the length of a stretcher fiber (inverse dispersion fiber with a dispersion parameter of -41 fs/nm/m at 1560 nm) in order to satisfy (c). An optimum length of 100 m is sufficient to cancel the dispersion offered by the CVBG and the rest of the components before frequency up-conversion. Prior to high-power amplification, pulses are passed through a circulator which first directs the laser pulses towards the CFBG and then to the 10 W EDFA.

Management of the entire dispersion in the stretcher

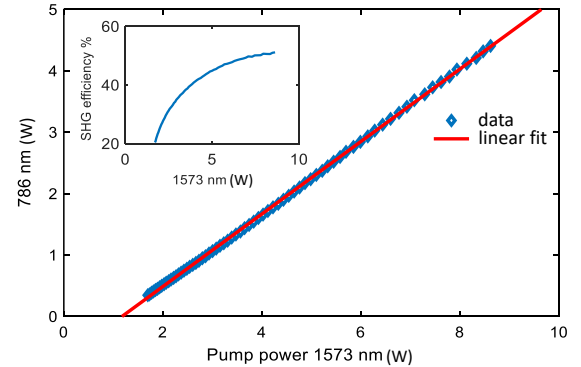


FIG. 4: Single-pass frequency conversion curve of the first doubling stage (1572 nm to 786 nm). The inset shows the frequency conversion efficiency curve with respect to pump power.

fiber is not possible due to the short pulse period of 200 ps which is similar to the pulse length of the stretched pulses. As a result, the pulse wings would overlap and we would forfeit the ability to separate the individual pulses for a clean pulse switching. Therefore, it is critical to distribute chirping in the system. The amplified (9.6 W average power) pulses are collimated and steered into the CVBG which reflects more than 90% of light. Temperature tuning of the CFBG enables us to precisely tune the dispersion by about  $\pm 0.005$  ps/nm to achieve compressed 560 fs pulses. The time-bandwidth product is measured to be 0.49, fairly close to a transform-limited pulse with a Gaussian pulse profile. We get 90% efficiency in the compressor and hence 8.6 W average power is available for frequency up-conversion out of the pulse compressor.

### B. Pump pulse energy optimization

Our goal is to at least double the UV pulse energy compared to the previously available  $\sim 80$  pJ [20]. With the given fundamental pump power of 8.6 W we did not succeed to significantly increase the pulse energy ( $\geq 160$  pJ) without lowering the repetition rate. We therefore block three out of every four pulses, thereby dropping the repetition rate of the idle signal by a factor of four, and increasing the pump pulse energy by the same factor. We stop here because a further drop ( $< 1.25$  GHz) in the repetition rate demands additional dispersion to avoid nonlinear pulse distortion during chirped pulse amplification. The speed of the gate operation scales with the repetition rate, therefore the payload repetition rate is kept unchanged. However, to satisfy the pulse energy requirement at 5 GHz repetition rate, we artificially retain the enhanced pulse energy in the payload pulses due to a relatively long time (hundreds of ns), which the 10 W amplifier takes to fully settle to a new steady state after a change in the repetition rate, shown in Fig. 5. We intentionally place the payload pulses at the start of

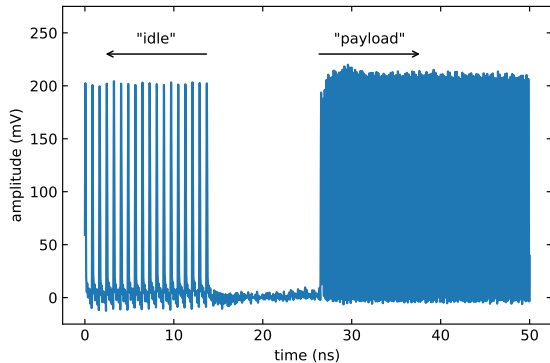


FIG. 5: Fast photodiode trace of laser pulses where the idle pulses have a 1.25 GHz repetition rate and the payload pulses have 5 GHz. The change in the repetition rate changes the steady state of the 10 W amplifier, i.e., it changes the pulse energy, but not the average power. Before this change starts to happen, the pulse amplitude remains the same for at least 150 ns (only partially shown), or for 750 consecutive pulses at 5 GHz. During this time and in this case, the average power is increased by a factor of 4 as compared to idle pulses.

this new steady state transition.

Under these conditions, vertically polarized 7 nJ laser pulses are focused down to 11  $\mu\text{m}$  spot size (@  $1/e^2$  radius) inside the periodically poled lithium niobate crystal to achieve a maximum peak intensity of 3  $\text{GW}/\text{cm}^2$ . The crystal is mounted inside a thermoelectric oven to achieve phase matching. As a result, we get over 4.3 W of average power at 786 nm which corresponds to a pulse energy of 3.5 nJ and a single-pass conversion efficiency of 50% as shown in Fig. 4.

### C. UV pulse energy estimation

The entangling gate operation requires only a few UV pulses at a high repetition rate which allows us to overcome thermal effects due to absorption inside the non-linear crystal. Hence, we can make a trade-off and favor a higher non-linear coefficient over a wide UV transparency range and choose non-critically phase-matched periodically poled potassium titanyl phosphate (PPKTP) instead of a conventional borate family crystal to generate 393 nm pulses.

For a pump power of 500 mW at 786 nm and 1.25 GHz repetition rate we get over 100 mW of 393 nm light focused to a spot size with a  $1/e^2$  radius of 8.5  $\mu\text{m}$ . Cross-correlation frequency-resolved optical gating measurement gives a UV pulse duration on the order of a picosecond. At higher pump intensities thermal-dephasing induced power fluctuations in the PPKTP crystal become problematic, as reported in earlier studies [24, 25]. As a consequence, it is difficult to gauge the exact power at the crystal output. Therefore, at a higher pump power, the duty cycle  $D_C$  of the pump beam has to be reduced

to get a stable output-power reading for pulse energy estimation. We choose a period  $T = 1$  ms and different pulse widths  $PW$  which yield  $D_C = PW/T$ . We use three different ways to measure the pulse energy. The measurements agree with each other with deviations of a few percent. First, for several different  $D_C \leq 1/1000$ , we measure the average UV power at maximum pump power and estimate a UV power  $\geq 1$  W. We verify the method by measuring (1) the minimum pump power, (2) the maximum pump power, (3) the UV power at minimum pump power, each with and without duty cycle—i.e.,  $D_C \ll 1$  and  $D_C = 1$ , respectively—and find an excellent agreement between actual and projected power numbers. Second, we use only a payload which comprises 50 pulses every 1 ms and get  $\sim 50$   $\mu\text{W}$  average power, which corresponds to  $\sim 5$  W of average power for a continuous pulse train at 5 GHz. The reason behind this huge power is a sudden increase in the repetition rate (5 GHz) of payload pulses while the amplifier is being operated in the steady state of 1.25 GHz. This also corroborates that the UV power with a continuous pulse train at 1.25 GHz is over 1 W. Third, we monitor the payload signal with a fast photodiode and oscilloscope to further verify the change in the pulse amplitude with the pump power. We find that the amplitude of the peak photodiode voltage grows steadily from 4 mV (100 mW UV power) to a maximum of 45 mV, which thus also corresponds to a UV power of  $\geq 1$  W. The fractional peak-to-peak amplitude noise is below 5%. For the given UV average power we determine a pulse energy  $\geq 800$  pJ even for a payload repetition rate of 5 GHz.

## V. FAST GATE SIMULATIONS

The experimental setup described in [20] combined with the ultrafast pulsed laser source based on a frequency comb presented above constitute the basis for the implementation of a fast two-qubit phase gate [26]. We propose an implementation using  $^{40}\text{Ca}^+$  ions where the qubit is stored in the  $4S_{1/2}$  and  $3D_{5/2}$  internal states and we use the  $4S_{1/2} \leftrightarrow 4P_{3/2}$  transition for applying state-dependent momentum kicks to the ions via resonant laser pulses. Two trapped ions loaded in a common 1D harmonic potential of frequency  $\omega$  freely evolve under the Hamiltonian  $H_0 = \hbar\omega_c a_c^\dagger a_c + \hbar\omega_s a_s^\dagger a_s$  with  $\omega_c = \omega$  and  $\omega_s = \omega\sqrt{3}$  and  $a_{c,s}^\dagger$  ( $a_{c,s}$ ) the creation (annihilation) phonon operator for the center-of-mass and stretch modes. This free evolution is interleaved with a fast pulsed interaction with an on-resonant laser beam kicking the ion described by  $H_1 = \Omega(t)[\sigma_1^\dagger e^{i\hbar kx_1} + \sigma_2^\dagger e^{i\hbar kx_2} + \text{H.c.}]/2$  with  $\sigma_i^\dagger$  the ladder spin operator for the  $i$ -th ion [6, 8, 27], and  $\Omega(t)$  is the Rabi frequency. The pulse duration  $\delta t$  and the pulse period are orders of magnitude faster than the trap period to fully excite and quickly de-excite the population via stimulated emission, i.e.  $\int_0^{\delta t} \Omega(\tau) d\tau = \pi$ . Additionally, each pulse is split

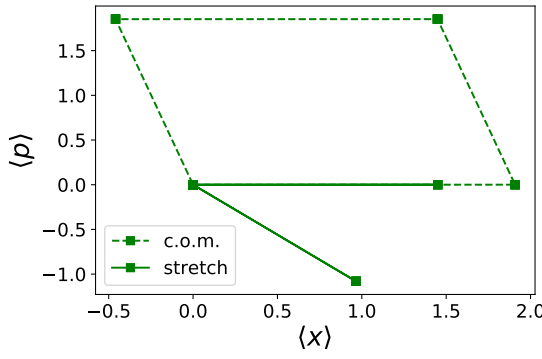


FIG. 6: Phase-space trajectory of the center of mass (dashed) and stretching (solid) modes in the frame of reference that rotates with the frequency of each mode  $\langle ae^{i\omega_{c,s}t} \rangle = (\langle x_{c,s} \rangle + i\langle p_{c,s} \rangle)/\sqrt{2}$  for a gate implemented by a sequence with 4 pulses. Only the center-of-mass motion contributes to the total phase  $\phi$  in this particular gate.

by a 50/50 beam splitter such that the resulting two pulses counter-propagate arriving at the ion with a relative delay  $\tau$ , controlled by the relative length of the two optical paths. In this manner, both the length of the pulses  $\delta t$  and the delay  $\tau$  between counter-propagating pulses are shorter than the lifetime of the  $4P_{3/2}$  state,  $\delta t, \tau \ll t_\gamma = 6.9$  ns. As consequence of the  $\hat{H}_1$  interaction the ion is excited by the first pulse acquiring a momentum  $\pm\hbar k$ . The second pulse coming from the opposite direction coherently de-excites the ion, providing the same amount of momentum  $\pm\hbar k$ . As discussed below, spontaneous emission during two consecutive pulses will define the ultimate fidelity that can be achieved in the resonant excitation scheme. Finally, the repetition rate of the laser is considered to be much faster than the trap frequency, allowing a fine-grained control of the pulse sequences.

The unitary generated by a sequence containing  $N$  pulses expressed in the center-of-mass and stretch coordinates takes the form  $\mathcal{U} = \mathcal{U}_c \mathcal{U}_s$ , where  $\mathcal{U}_{c,s} = \prod_{n=1}^N U_{c,s}(t_n)$  are the unitary operators produced by  $H_1$  and an interspersed free evolution  $H_0$  during a  $t_n$  time [26]. In phase space, the Heisenberg representation allows us to interpret these interactions as displacements of the Fock operators  $a_{c,s}$  by a complex number  $A_{c,s}$  that depends on the collective state of the ions

$$\begin{aligned} a_c \rightarrow a_c + A_c &= a_c + i(\sigma_1^z + \sigma_2^z)\alpha_c \sum_n e^{-i\omega_c t_n}, \\ a_s \rightarrow a_s + A_s &= a_s + i(\sigma_1^z - \sigma_2^z)\alpha_s \sum_n e^{-i\omega_s t_n}, \end{aligned} \quad (1)$$

with strengths  $\alpha_c = \eta/2^{3/2}$  and  $\alpha_s = \alpha_c/3^{1/4}$  proportional to the Lamb-Dicke parameter  $\eta = k\sqrt{\hbar}/(2m\omega)$ . The normal modes follow polygonal orbits, see Fig. 6, where the edges all have uniform length  $\sim \alpha_{c,s}$  and controllability of the kicking sequence is limited to the allo-

cation of the pulse arrival times  $\omega t_n$  that determines the relative angle between edges. In case that both modes restore the initial position in phase-space,

$$A_c = A_s = 0, \quad (2)$$

the resulting unitary is equivalent to a free evolution up to a global phase, which is independent of the motional states

$$\phi = \alpha_c^2 \sum_{j=2}^N \sum_{k=1}^{j-1} \left[ \frac{\sin(\sqrt{3}\omega t_{jk})}{\sqrt{3}} - \sin(\omega t_{jk}) \right], \quad (3)$$

with  $t_{jk} = t_j - t_k$ . When this phase becomes

$$\phi = \pi/4 + 2n\pi \quad n = 0, 1, 2 \dots \quad (4)$$

the free evolution corresponds to a controlled-phase gate.

In the following we solve the set of equations (2) and (4). The fastest allowed gate will depend on the controllability degree, however, this simple scenario which relies only on pulse picking [26], and fixes the strength, direction, and repetition rate of the pulses, leads to gates faster than the trapping period  $T < 2\pi/\omega$ . Due to the finite repetition rate of the source generator, the pulse sequence design combines *i*) simple continuous solutions with *ii*) fine-tuned pulse picking based on a genetic algorithm [26] leading to optimal solutions that minimize the gate error  $\epsilon = |A_c|^2 + |A_s|^2$  that quantifies the deviations to recover the original position after the whole kicking sequence.

The fastest sequence fulfilling Eqs. (2) and (4) corresponds to a sequence of 4 pulses and a trapping frequency of  $\omega \sim 2\pi \times 0.27$  MHz. The resulting phase gate is implemented in a time  $T \sim 0.79 \times 2\pi/\omega$ , assuming a repetition rate of  $\sim 5$  GHz. The phase-space trajectories of the center-of-mass and stretching modes for such gate are depicted in Fig. 6.

In these protocols, the motional state of the ion is almost perfectly restored and the gate fidelity is fundamentally limited by the errors in the internal state of the ion. More precisely, our method for kicking the ion implies that the atom spends some time in the excited state  $4P_{3/2}$ . We can safely assume short pulses with a duration  $\tau \simeq 1$  ps and a spacing  $t_{\text{wait}} \simeq 1$  ps much shorter than the inverse of the spontaneous emission rate  $1/\gamma \simeq 7$  ns. Under these conditions, the probability that the ion relaxes, emitting a photon, is essentially  $\epsilon_1 \sim \mathcal{O}(\gamma t_{\text{wait}}) \sim 1.8 \times 10^{-4}$ . If we have a sequence of  $N$  kicks, the infidelity of the gate operation is approximately  $\epsilon_N = 1 - (1 - \epsilon)^N \sim \mathcal{O}(N t_{\text{wait}} \gamma)$  or  $\epsilon_4 \simeq 7.4 \times 10^{-4}$  for the optimal sequence described above.

This error can be decreased using shorter pulses or substituting the resonant  $4S_{1/2} \leftrightarrow 4P_{3/2}$  transition, with a Raman or STIRAP process that connects the qubit states  $4S_{1/2} \rightarrow 3D_{5/2}$ . The energy difference between S and D states is still sufficiently large such that a single transition will impart a significant momentum to the ion. However, the spontaneous decay rate of the D ( $\sim 1.1$  s) is

orders of magnitude smaller, eliminating the fundamental limitation due to spontaneous emission.

Note that faster gates, acting on a time  $T \sim 0.25 \times 2\pi/\omega$  have been recently designed [28]. However, this theoretical limit remains a technical challenge, because it requires switching the directions of the laser pulses—i.e. choice of which pulse arrives first in the counter-propagating pair—, a process that may induce additional sources of error and deteriorate the gate fidelity [10]. Another approach based on pulse shaping techniques has produced optimal continuous protocols [11] with fast experimental gates of around  $T \sim 0.89 \times 2\pi/\omega$ , but they still exhibit a rather poor fidelity of 0.6.

## VI. CONCLUSION AND OUTLOOK

Bursts of UV pulses at 5 GHz repetition rate with an average power of 5 W have been reported, while keeping the bandwidth small ( $\sim 500$  GHz). The resulting pulse energy is  $\sim 10$  times higher than the previous demonstra-

tion for a coherent population transfer in a  $^{40}\text{Ca}^+$  ion. This will enable us to create a pulse pair from a single pulse to generate  $2\hbar k$  momentum kicks for the implementation of fast entangling gate operations.

An addition of the linear chirp in the UV pulses can implement adiabatic rapid passage, that can make coherent excitations robust against pulse intensity fluctuations [29]. The enhanced pulse energy will allow us to overcome the losses while adding a required linear chirp in the pulses.

## Acknowledgments

We acknowledge support from Project PGC2018-094792-B-I00 (MCIU/AEI/FEDER,UE), CSIC Research Platform PTI-001, and CAM/FEDER Project No. S2018/TCS-4342 (QUITEMAD-CM). Additionally, we acknowledge funding by the Institut für Quanteninformation GmbH.

---

[1] F. Schmidt-Kaler, H. Häffner, M. Riebe, S. Gulde, G. P. Lancaster, T. Deusdle, C. Becher, C. F. Roos, J. Eschner, and R. Blatt, *Nature* **422**, 408 (2003).

[2] S. Gulde, M. Riebe, G. P. Lancaster, C. Becher, J. Eschner, H. Häffner, F. Schmidt-Kaler, I. L. Chuang, and R. Blatt, *Nature* **421**, 48 (2003).

[3] H. Häffner, C. F. Roos, and R. Blatt, *Phys. Rep.* **469**, 155 (2008).

[4] T. Harty, D. Allcock, C. J. Ballance, L. Guidoni, H. Janacek, N. Linke, D. Stacey, and D. Lucas, *Phys. Rev. Lett.* **113**, 220501 (2014).

[5] T. Monz, D. Nigg, E. A. Martinez, M. F. Brandl, P. Schindler, R. Rines, S. X. Wang, I. L. Chuang, and R. Blatt, *Science* **351**, 1068 (2016).

[6] J. I. Cirac and P. Zoller, *Phys. Rev. Lett.* **74**, 4091 (1995).

[7] K. Mølmer and A. Sørensen, *Phys. Rev. Lett.* **82**, 1835 (1999).

[8] J. J. García-Ripoll, P. Zoller, and J. I. Cirac, *Phys. Rev. Lett.* **91**, 157901 (2003).

[9] W. Campbell, J. Mizrahi, Q. Quraishi, C. Senko, D. Hayes, D. Hucul, D. Matsukevich, P. Maunz, and C. Monroe, *Phys. Rev. Lett.* **105**, 090502 (2010).

[10] J. Mizrahi, C. Senko, B. Neyenhuis, K. Johnson, W. Campbell, C. Conover, and C. Monroe, *Phys. Rev. Lett.* **110**, 203001 (2013).

[11] V. Schäfer, C. Ballance, K. Thirumalai, L. Stephenson, T. Ballance, A. Steane, and D. Lucas, *Nature* **555**, 75 (2018).

[12] C. Zhang, F. Pokorny, W. Li, G. Higgins, A. Pöschl, I. Lesanovsky, and M. Hennrich, *Nature* **580**, 345 (2020).

[13] J. D. Wong-Campos, S. A. Moses, K. G. Johnson, and C. Monroe, *Phys. Rev. Lett.* **119**, 230501 (2017).

[14] G. Samanta, S. C. Kumar, A. Aadhi, and M. Ebrahim-Zadeh, *Opt. Express* **22**, 11476 (2014).

[15] F. Emaury, A. Diebold, C. J. Saraceno, and U. Keller, *Optica* **2**, 980 (2015).

[16] H. Wang, Y. Xu, S. Ulonska, J. S. Robinson, P. Ranitovic, and R. A. Kaindl, *Nat. Commun.* **6**, 7459 (2015).

[17] N. A. Chaitanya, A. Aadhi, M. Jabir, and G. K. Samanta, *Opt. Lett.* **40**, 4269 (2015).

[18] F. Köttig, F. Tani, C. M. Biersach, J. C. Travers, and P. S. J. Russell, *Optica* **4**, 1272 (2017).

[19] M. I. Hussain, M. J. Petrasunas, C. D. Bentley, R. L. Taylor, A. R. Carvalho, J. J. Hope, E. W. Streed, M. Lobino, and D. Kielpinski, *Opt. Express* **24**, 16638 (2016).

[20] D. Heinrich, M. Guggemos, M. Guevara-Bertsch, M. I. Hussain, C. F. Roos, and R. Blatt, *New J. Phys.* **21**, 073017 (2019).

[21] A. McCoy, L. Fu, M. Ibsen, B. Thomsen, and D. Richardson, *Electron. Lett.* **40**, 107 (2004).

[22] D. Heinrich, Ph.D. thesis, University of Innsbruck (2020).

[23] R. Bonk, *Linear and nonlinear semiconductor optical amplifiers for next-generation optical networks* (KIT Scientific Publishing, 2013).

[24] J. H. Lundeman, O. B. Jensen, P. E. Andersen, and P. M. Petersen, *Appl. Phys. B* **96**, 827 (2009).

[25] Y. Han, X. Wen, J. Bai, B. Yang, Y. Wang, J. He, and J. Wang, *J. Opt. Soc. Am. B* **31**, 1942 (2014).

[26] E. Torrontegui, D. Heinrich, M. I. Hussain, R. Blatt, and J. J. García-Ripoll (arXiv:2007.00734).

[27] J. J. García-Ripoll, P. Zoller, and J. I. Cirac, *Phys. Rev. A* **71**, 062309 (2005).

[28] E. P. G. Gale, Z. Mehdi, L. M. Oberg, A. K. Ratcliffe, S. A. Haine, and J. J. Hope (2019), arXiv:1912.07780.

[29] V. Malinovsky and J. Krause, *Eur. Phys. J. D* **14**, 147 (2001).